Impact of Edge–Core Structures and Substituent Effects on the Electronic and Charge-Transport Properties of Heteroaromatic Ring-Fused Oligomers

ARTICLE *in* THE JOURNAL OF PHYSICAL CHEMISTRY C · JANUARY 2015

Impact Factor: 4.77 · DOI: 10.1021/jp5086922

4 AUTHORS, INCLUDING:

Jin-Dou Huang

Chinese Academy of Sciences

15 PUBLICATIONS **166** CITATIONS

THE JOURNAL OF PHYSICAL CHEMISTRY C

Article

pubs.acs.org/JPCC

Impact of Edge-Core Structures and Substituent Effects on the Electronic and Charge-Transport Properties of Heteroaromatic Ring-Fused Oligomers

Jin-Dou Huang,[†] Shuo Chai,[§] Huipeng Ma,*[,‡] and Bin Dong*[,†]

[†]School of Physics and Materials Engineering, Dalian Nationalities University, Dalian 116600, China

[‡]College of Medical Laboratory Science, Dalian Medical University, Dalian 116044, China

[§]School of Physics and Optoelectronic Technology, Dalian University of Technology, Dalian 116024, China

Supporting Information

ABSTRACT: Herein, we systematically studied the electronic and conducting properties of the thiophene-fused polycyclic aromatic compounds and their analogues and discussed in detail the influences of edge-core structure, heteroatom substitution, and functionalization on their field-effect transistor properties and solid-state packing motifs. It was found that the influence of edge-core structure and heteroatom substitution on the electronic properties and reorganization energies of semiconducting materials mainly originates from the variations of the frontier molecular orbital charge distributions and the steric hindrance as well as the conjugate degree of compounds. Moreover, our results also showed that the fusion of benzene rings at the longitudinal end could effectively decrease energy barrier of charge injection and reorganization energies and change the molecular arrangement from herringbone packing to π stacking, which provides a promising way to functionalize organic semiconducting molecules.

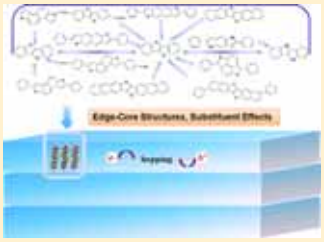

1. INTRODUCTION

Organic semiconductors have received much attention in organic electronics research, particularly in device applications, such as organic light-emitting diode (OLED),[1] organic field-effect transistors (OFETs),[2] and organic photovoltaic (OPV) devices.[3] For these applications, the performance of the electronic device largely depends on the charge-transport properties of organic materials, therefore, the exploration of new organic materials with high carrier mobility and good air stability, and further understanding of the detailed structure−property relationships is essential for improvement of device performance.

Recently, the benzothieno[3,2-*b*][1]-benzothiophene (BTBT) and their derivatives/analogues, as a class of new building blocks for organic semiconducting materials, have been successfully synthesized and their utility as active layers for OFETs was widely investigated.[4−12] For example, Takimiya et al. synthesized and characterized the dianthra[2,3-b:2′,3′-f]thieno[3,2-*b*]thiophene (**12**) and a field-effect mobility as high as 3.0 $cm^2 V^{-1} s^{-1}$ was achieved, even though the thin-film ordering in the OFET is not very good;[9] subsequently, the same research group reported another BTBT derivative, diphenyl-dinaphtho[2,3-b:2′,3′-f]-thieno[3,2-*b*]thiophene (**13**), and the corresponding OFETs showed typical p-channel transistor characteristics with mobility of as high as 3.5 $cm^2 V^{-1} s^{-1}$.[11] In 2011, the analogues of BTBT, including the linear- and angular-shaped naphthodithiophenes, were exploited, and the OFET devices fabricated on the basis of these compounds (such as compound **14**) exhibited excellent FET performances, with remarkably high charge carrier mobility (1.5 $cm^2 V^{-1} s^{-1}$) and large current on/off ratios ($I_{on}/I_{off} = 10^7$).[8] Additionally, it is also worthwhile to mention that Mitsui et al. prepared the O-substituted angular-shaped naphthodithiophenes, such as compounds **3** and **4** (see Scheme 1), and analyzed the impact of heteroatom substitution on the crystal packing and intermolecular π-orbital overlap, which well-explained the high mobility of compounds **3** and **4**.[10] In comparison with current extensive experimental investigations, there have been few systemically theoretical studies on these thiophene/furan-fused polycyclic aromatic compounds, especially the relationship between the charge transport properties and molecular structures. In order to elucidate the structure−property relationships in organic electronic materials, we take BTBT and their derivatives/analogues as model systems to systematically investigate the influence of molecular structures on the physicochemical and semiconducting properties of organic semiconducting materials.

Herein, based on quantum-chemical calculations and Marcus−Hush theory, the electronic and conducting properties of BTBT and its derivatives/analogues (as shown in Scheme 1), were calculated in detail, and the influences of edge-core structure, heteroatom substitution, and functionalization on the FET properties of materials were systematically discussed in Edge-Core Structure Effects and Heteroatom and Substitutents Effects. Then, combined with analytical function of anisotropic mobility, we analyzed the anisotropy of the hole-transfer

Received: August 28, 2014
Revised: December 1, 2014
Published: December 5, 2014

DOI: 10.1021/jp5086922
J. Phys. Chem. C 2015, 119, 33−44

Scheme 1. Molecular Structures of Thiophene-Fused Polycyclic Aromatic Compounds and Their Derivatives/Analogues

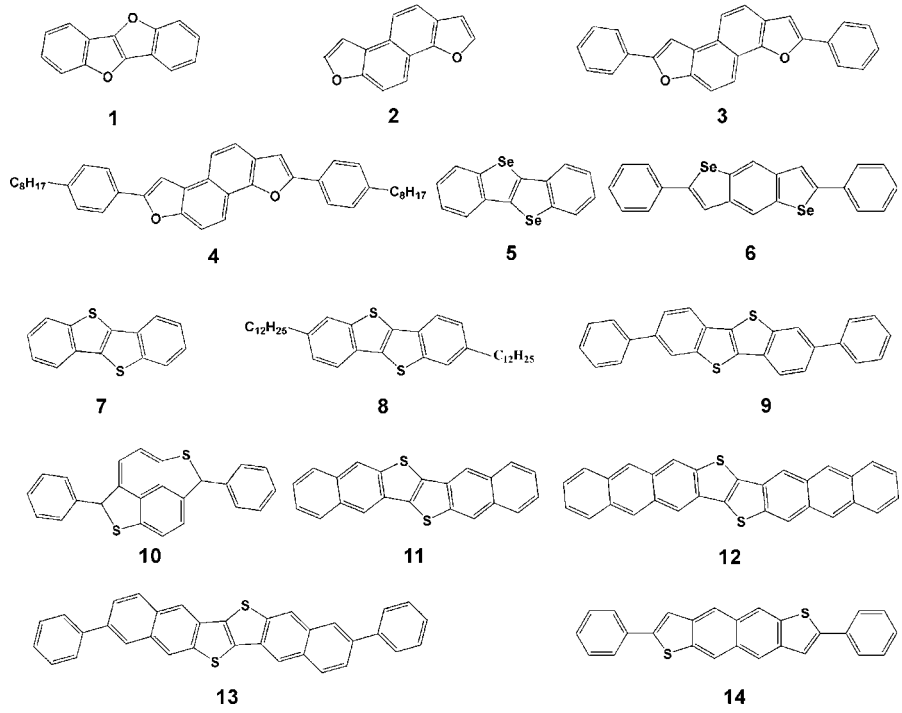

mobilities and electron-transfer mobilities and pointed out the optimal charge-carrier transport direction of the studied compounds in OFET device. Our theoretical investigations here provide not only a fundamental understanding of the influence of molecular modification on the material properties but also an effective theoretical guidance for the rational design of new derivatives with superior properties.

2. COMPUTATIONAL METHODS

As one of the most important factors that govern the intermolecular charge transfer process in organic materials, the reorganization energy is mainly related to the geometric relaxation of the molecule (inner reorganization energy) and its surroundings (outer reorganization energy) on movement of the charge carriers. In organic crystals, external reorganization energy is usually neglected because of the low dielectric constants of molecular solids, and fortuitous cancellation of errors that includes neglect of tunnelling contributions to the rate constants.[13,14] The inner reorganization energy λ associated with charge transport process in organic semiconducting materials can be evaluated in two ways. The first is the adiabatic potential-energy surface method, in which the λ can be expressed as follows:

$$\lambda = \lambda_1 + \lambda_2 = (E_{\pm}^{*} - E_{\pm}) + (E^{*} - E) \quad (1)$$

Here, E and $E_{\pm}$ represent the energies of the neutral and cation/anion species in their lowest-energy geometries, respectively; E^{*} and $E_{\pm}^{*}$ are the energies of the neutral and cation/anion species with the geometries of the cation/anion and neutral species, respectively. The other method is the normal-mode (NM) analysis method. The contribution of each vibrational mode to λ can be obtained by expanding the potential energies of the neutral and cationic/anionic states in a power series of the normal coordinates. In the harmonic approximation, the reorganization energy can be written as

$$\lambda = \Sigma\lambda_i = \Sigma(\omega_i \Delta Q_i^{2})/2 \quad (2,)$$

where ΔQ_i represents the displacement along normal mode Q_i between the equilibrium geometries of the neutral and charged molecules; ω_i is the corresponding frequency. The NM analysis and λ_i were obtained through the DUSHIN program.[15]

From the adiabatic potential-energy surfaces of neutral/charged species, the vertical ionization potential (VIP), adiabatic ionization potential (AIP), vertical electronic affinity (VEA), and adiabatic electron affinity (AEA) can be calculated as

$$\begin{aligned} \mathrm{VIP} &= E_{+}^{*} - E \\ \mathrm{AIP} &= E_{+} - E \\ \mathrm{VEA} &= E - E_{-}^{*} \\ \mathrm{AEA} &= E - E_{-} \end{aligned} \quad (3)$$

Full geometry optimizations of the monomer molecules and the energy calculations are carried out using the B3LYP functional in conjunction with the 6-311G** basis set. These calculations are performed with the Gaussian 03 package.[16]

The other key factor influencing the charger-transfer rate is intermolecular electronic couplings. In a symmetrically orthonormalized basis, the intermolecular electronic coupling V_{ij} takes the following form

$$V_{ij} = |(J_{ij} - 0.5*(e_i + e_j)*S_{ij})/(1 - S_{ij}^{2})| \quad (4)$$

Here, the spatial overlap (S_{ij}), charge transfer integrals (J_{ij}), and site energies (e_i, e_j) can be written as

$$e_{i(j)} = < \Psi_{i(j)}|H|\Psi_{i(j)}> \quad (5,)$$

$$S_{ij} = < \Psi_i|\Psi_j> \quad (6,)$$

DOI: 10.1021/jp5086922
J. Phys. Chem. C 2015, 119, 33−44

$$J_{ij} = <\Psi_i|H|\Psi_j> \quad (7,)$$

where H is the system Kohn−Sham Hamiltonian of the dimer system and $\Psi_{i(j)}$ means the monomer HOMOs (for hole transport) or LUMOs (for electron transport) with Löwdin's symmetric transformation which can be used as the orthogonal basis set for calculation. The calculations of all electronic couplings in different molecular dimers are performed with the PW91/QZ4P of density functional theory (DFT) implemented in the Amsterdam density functional (ADF) program.[17]

At room temperature, it is generally accepted that the charge-carrier transport in organic materials takes place via charge hopping between adjacent molecules. Assuming no correlation between charge hopping events and charge motion is a homogeneous random walk, the average drift mobility for charge carrier (hole/electron) transport in semiconductor materials can be simply written as

$$\mu = \frac{e}{k_B T} D = \frac{e}{k_B T} \lim_{t\to\infty} \frac{1}{2n} \frac{\langle x(t)^2 \rangle}{t} \approx \frac{e}{2nk_B T} \sum_i r_i^2 W_i P_i \quad (8)$$

where n is the spatial dimensionality, r_i is the hopping distance, P_i is the hopping probability, $P_i = W_i/\Sigma_i W_i$, i means the ith pathway, and W is the intermolecular hopping rate based on Marcus−Hush theory in the high-temperature limit:

$$W = \frac{V^2}{\hbar}\left(\frac{\pi}{\lambda k_B T}\right)^{1/2} \exp\left(-\frac{\lambda}{4k_B T}\right) \quad (9,)$$

λ is the reorganization energy and V is the intermolecular effective electronic coupling.

According to the fact that the magnitude of the field effect mobility in a particular transistor channel depends on the specific surface of the organic crystal and the orientation angle of the transistor channel relative to the reference axis, we proposed the orientation function in our previous studies, which establishes the quantitative relationship between angular resolution anisotropic mobility and molecular packing architecture parameters.[18−20] The basic prerequisite for the orientation function application is that the molecules in the basal stacked layers are central symmetric and there is no structural disorder in crystals. In fact, most ideal high-purity crystals meet the above demands, and their anisotropic hole/electron mobilities on the surface of organic crystals can be simulated though our orientation function. The orientation function describing the mobility in a specific conduction direction on a specific surface in organic crystals can be written as[18−24]

$$\mu_\Phi = \frac{e}{2k_B T} \sum_i W_i r_i^2 P_i \cos^2 \gamma_i \cos^2(\theta_i - \Phi) \quad (10)$$

where r_i is the hopping distance, $P_i \cos^2 \gamma_i \cos^2 (\theta_i - \Phi)$ describes the relative hopping probability of various electronic coupling pathways to the specific transistor channel; γ_i represents the angles between the charge hopping pathways and the plane of interest, and for the hopping paths in the basal stacked layers, the γ_i are 0 degrees; θ_i are the angles of the projected hopping paths of different dimer types relative to the reference axes, and their values can be determined by the molecular architecture in the organic crystal, as shown in Figure 1; Φ is the orientation angle of the transistor channel relative to the reference axis. Equation 10 can be considered as an anisotropic two-dimensional random walk with the charge drifting effect in one direction, and it provides an analytic function to determine the angular resolution anisotropic mobilities for layered organic semiconductors by relating the crystal packing and electron coupling V to the outer measuring channel angle Φ.

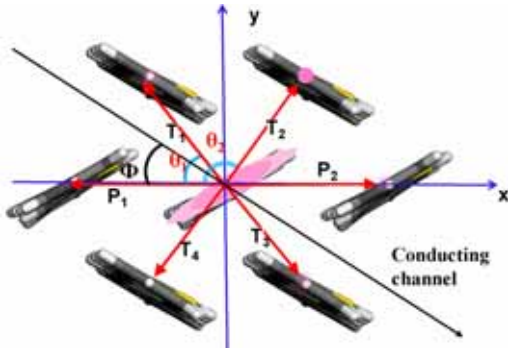

Figure 1. Different hopping paths projecting to a transistor channel in the basal stacked layers.

3. RESULTS AND DISCUSSION

3.1. Edge-Core Structure Effects. The ionization potentials (IPs) and electron affinities (EAs) are generally regarded as essential prerequisites for the rational design of new-type electronic materials due to the fact that they are related to the injection efficiency of holes/electrons into the HOMOs/LUMOs and the material stability under processing/ambient operating conditions.[23,25] Here, the adiabatic ionization potentials (AIPs), vertical ionization potentials (VIPs), adiabatic electron affinities (AEAs), and vertical electron affinities (VEAs) for the compounds **1**, **2**, **9**, **10**, and **14** are summarized in Table 1. Compound **1** is the isomeric compound of **2**, and both of them show high aromaticity. The similar conjugated chain lengths result in the relatively small differences in their IPs and EAs. Further analysis indicates that molecule **1** has the slightly higher IP and EA values than molecule **2**, which mainly derives from their different edge-core

Table 1. Calculated Vertical Ionization Potential (VIP), Adiabatic Ionization Potential (AIP), Vertical Electronic Affinity (VEA), and Adiabatic Electron Affinity (AEA) for the Compounds 1−14

molecular crystals	VIP (eV)	AIP (eV)	VEA (eV)	AEA (eV)	HOMO−LUMO gap (eV)
1	7.391	7.239	−0.149	−0.009	4.38
2	7.276	7.176	−0.265	−0.122	4.33
3	6.593	6.506	0.573	0.681	3.59
4	6.389	6.299	0.531	0.634	3.56
5	7.238	7.142	0.128	0.280	4.14
6	6.759	6.636	0.822	0.944	3.43
7	7.336	7.223	0.043	0.195	4.27
8	6.960	6.837	0.028	0.182	4.25
9	6.868	6.741	0.601	0.785	3.86
10	6.223	6.141	1.073	1.289	2.64
11	6.685	6.619	0.833	0.936	3.35
12	6.213	6.169	1.413	1.484	2.64
13	6.469	6.395	1.099	1.207	3.18
14	6.449	6.374	0.927	1.098	3.40

DOI: 10.1021/jp5086922
J. Phys. Chem. C 2015, 119, 33−44

structures, as shown in Scheme 1. In the molecule **1**, the core part is fused furans and two benzene units are fused to both termini of fused furan core. In molecule **2**, the furan rings are fused to either termini of the naphthalene core. The difference in the sequence arrangement of aromatic rings leads to different HOMO/LUMO distributions. Figure 2 depicts the HOMO

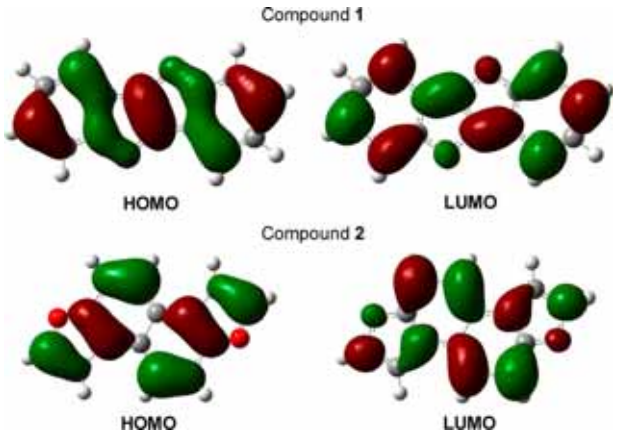

Figure 2. HOMOs (0.025 au) and LUMOs (0.025 au) for compound **1** (top) and **2** (bottom).

and LUMO distributions of compounds **1** and **2**. Comparison of HOMOs of compounds **1** and **2** shows that there are more bonding relationships between neighboring atoms in HOMO of compound **1** than in HOMO of compound **2**. In other words, the local bonding character in the HOMO of compound **1** includes more bonding fashion, which is beneficial for the reduction of HOMO energy. Besides, the HOMO of molecule **1** also includes more 2p orbitals of O, whose energy is slightly lower than C atomic 2p orbital energy, and thus the position of HOMO further shifts to a lower energy. Different from bonding character in HOMOs, the LUMOs of compounds **1** and **2** both show strong antibonding character, and the percentage of antibonding character is smaller in the LUMO of compound **1** than in the LUMO of compound **2**, which well-explains the relatively low EA value of compound **1** in comparison with compound **2**. As shown in Table 1, the HOMO−LUMO gap of compound **1** (4.38 eV) is almost the same with that of compound **2** (4.33 eV), due to the similar difference in IP values of molecules **1** and **2** with the difference in their EA values. It suggests that the variation of edge-core structure has little influence on the photo absorption performance of materials.

For the isomeric compounds **9** and **14**, the order of IP values is completely opposite to the order of EA values, which is different from compounds **1** and **2**. The VIP and VEA values for compound **9** are separately 6.868 and 0.601 eV, which is larger and smaller than the corresponding VIP (6.449 eV) and VEA (0.927 eV) values of compound **14**, respectively. It is consistent with the larger HOMO−LUMO gap of compound **9** (3.86 eV) than that of compound **14** (3.40 eV), as shown in Table 1. Previous experimental and theoretical studies showed that the HOMO level increases, while the LUMO level and the HOMO−LUMO gap decrease as the conjugated chain length is elongated.[23,26,27] The above differences in VIP values, EA values, and HOMO−LUMO gaps are also associated with the smaller effective conjugation length of compound **9** than compound **14**. In compound **9**, the steric effect between the H atoms in bilateral and core phenyl groups induces large dihedral angles between the bilateral benzene rings and the molecular core plane (α = 40.2°), which decrease effective conjugation length along long molecular axis. In comparison, although the steric effect between the H atoms also influence conjugate degree of compound **14**, the attractive interaction between H and S atoms overcomes the steric hindrance to some extent and increases the planarity of the whole molecule (α = 29.4°) and thus results in relatively large effective conjugation length along the long molecular axis. In the terms of frontier molecular orbitals, the percentage of bonding character is significantly larger in the HOMO of compound **9** than in the HOMO of compound **14** (see Figure 3), which leads to the lower HOMO

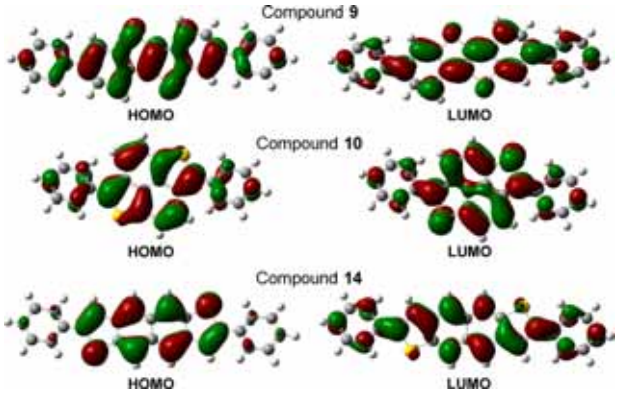

Figure 3. HOMOs (0.025 au) and LUMOs (0.025 au) for compounds **9** (top), **10** (middle), and **14** (bottom).

energy level and the larger IP value of **9**. For the LUMOs of compounds **9** and **14**, their bilateral phenyl groups (edge part) show very similar local bonding characters, while the core part shows some different bonding characters. The most important ones are as follows: (i) the local bonding character of compound **9** includes more antibonding fashion compared with compound **14** and (ii) the LUMO localized on the core of molecule **9** includes more 3p orbitals of S atom, whose energy is much higher than C atomic 2p orbital energy. These factors contribute to the higher LUMO energy level and lower EA values of **9**. As an analogue of molecule **9** and **14**, compound **10** also includes four benzene rings and two thiophene rings, but it shows higher C/H ratio than molecules **9** and **14** due to its distinctive aromatic core structure. Interestingly, molecule **10** with the square-shaped core structure shows higher IP value (6.223 eV), lower EA value (1.073 eV), as well as the smaller HOMO−LUMO gap (only 2.64 eV) than the linear-shaped **9** and **14**. It may be related to the higher conjugation degree of square-shaped aromatic core structure.

Table 2 collects the reorganization energies (λ) of the compounds **1**, **2**, **9**, **10**, and **14**. The calculation results show that the λ values estimated from the adiabatic potential energy surface of neutral/charged molecule (the four-point approach) agree well with those from the mode-specific method. The compound **14** is an exception, where the reorganization energy for electron-transfer (λ_e) evaluated from the four-point approach (0.304 eV) is smaller than that evaluated from normal-mode analysis (0.347 eV). It may be attributed to the limitation of harmonic approximation.

For the isomeric compounds **1** and **2**, the reorganization energies associated with the electron-transport process (λ_e) are

DOI: 10.1021/jp5086922
J. Phys. Chem. C 2015, 119, 33−44

Table 2. Internal Reorganization Energies Associated with Intermolecular Hole-Transfer and Electron-Transfer for Compounds 1−14 are Evaluated from the Adiabatic Potential-Energy Surface Method and Normal-Mode (NM) Analysis Method

	reorganization energies (hole) eV		reorganization energies (electron) eV	
molecular crystals	normal mode	adiabatic potential	normal mode	adiabatic potential
1	0.307	0.303	0.286	0.283
2	0.207	0.205	0.287	0.285
3	0.177	0.176	0.214	0.217
4	–	0.182	–	0.208
5	0.198	0.197	0.305	0.303
6	0.263	0.254	0.249	0.249
7	0.231	0.229	0.305	0.303
8	–	0.248	–	0.301
9	0.250	0.249	0.354	0.355
10	0.162	0.161	0.382	0.389
11	0.136	0.134	0.208	0.206
12	0.089	0.089	0.144	0.143
13	0.149	0.149	0.218	0.218
14	0.158	0.156	0.347	0.304

nearly the same (0.286 eV for **1** and 0.287 eV for **2**) due to their similar plane rigidity and LUMO distribution shape. The detail analysis of mode-specific reorganization energies for compounds **1** and **2** shows that the vibrational mode distributions of compounds **1** and **2** show some different characters, although the contributions of the vibration modes to λ_e mainly come from high-frequency modes for both compounds **1** and **2**. Figure 4 displays the frequency dependence of mode-specific reorganization energies for compounds **1** and **2**. We can see that the contributions to the electron-transfer reorganization energy of both compounds **1** and **2** mainly come from high-frequency modes above 1000 cm^{-1}: 79.4% of the total relaxation energy of compound **1** originates from vibrational modes at about 1000 cm^{-1} or higher, and 78.0% of the relaxation energy of compound **2** involves vibrational modes above 1000 cm^{-1} or higher. The further analysis shows that most of these high-frequency modes are associated with the stretching vibration of chemical bonds in middle part of the molecules. The largest contribution to the λ_e of compound **1** mainly come from the vibration modes at 1665 cm^{-1} in neutral state (0.068 eV) and at 1646 cm^{-1} in the anion state (0.084 eV), which corresponds to the stretching vibration of CC bonds of the center thiophene rings along the long molecular axis. Similarly, the 1609 cm^{-1} mode in the anion state (0.051 eV) and the 1756 cm^{-1} mode in the neutral state (0.034 eV), which have largest contributions to the total λ_e of compound **2**, correspond to the stretching vibration of CC bonds of the center benzene rings along the long molecular axis. Moreover, the low-frequency modes (<600 cm^{-1}) also contribute to the λ_e of compounds **1** and **2**, but the contributions to compound **2** are much more than to compound **1**: 18.8% of the relaxation energy comes from low-frequency modes below 600 cm^{-1}; in contrast, the contributions of the low-frequency modes to the electron-transfer reorganization energy of compound **1** only occupy 6.3%. For compound **2**, the low-frenquency vibration modes (311, 319, 413, and 419 cm^{-1}), making large contributions to the total λ_e, mainly come from the bending vibrations of center benzene rings; in contrast, the bending vibrations of center thiophene and bilateral benzene rings contribute very little to the λ_e of compound **1**.

The reorganization energies associated with the hole-transport process (λ_h) are significantly different for compounds **1** and **2**, which are in sharp contrast with their λ_e values. The λ_h value for compound **2** is about 0.205 eV, almost 0.1 eV smaller than the λ_h value for compound **1**. Comparison of their HOMO distributions shows that the HOMO of compound **2** has stronger nonbonding character than that of compound **1**, as shown in Figure 2. Considering that nonbonding does not cause change in bond order and induces much less bond length adjustment than bonding and antibonding types upon hole transfer, it rationalizes the observation that the λ_h value for compound **2** is much smaller than the one for compound **1**. The frequency analysis also shows that the stretching vibration of CC bonds, especially the CC bond in the center of the molecular core, contribute much less to compound **2** than to **1**. For example, the 1649 cm^{-1} mode in the cation state and the 1631 cm^{-1} mode in the neutral state, which are associated with the stretching vibration of center CC bonds along short

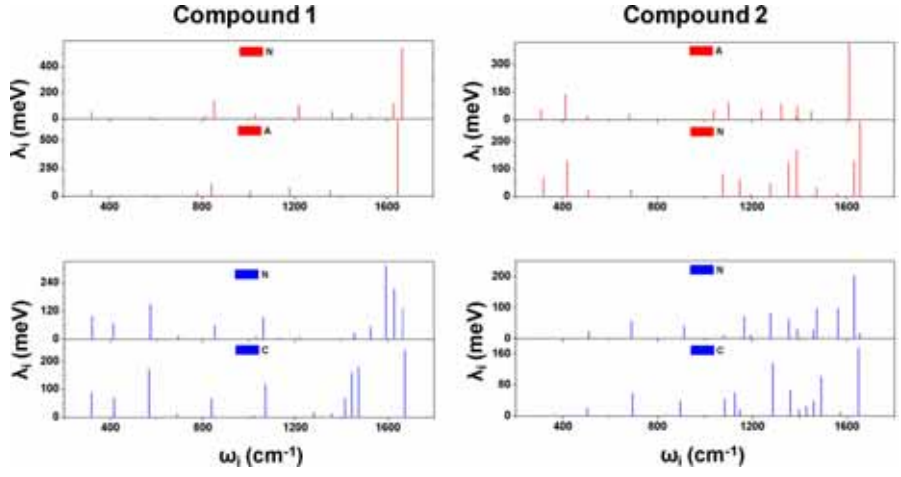

Figure 4. Frequency dependence of reorganization energies for neutral/anionic compound **1** (left) and **2** (right) upon the electron-transfer process and for neutral and cationic compound **1** (left) and **2** (right) upon the hole-transfer process.

DOI: 10.1021/jp5086922
J. Phys. Chem. C 2015, 119, 33−44

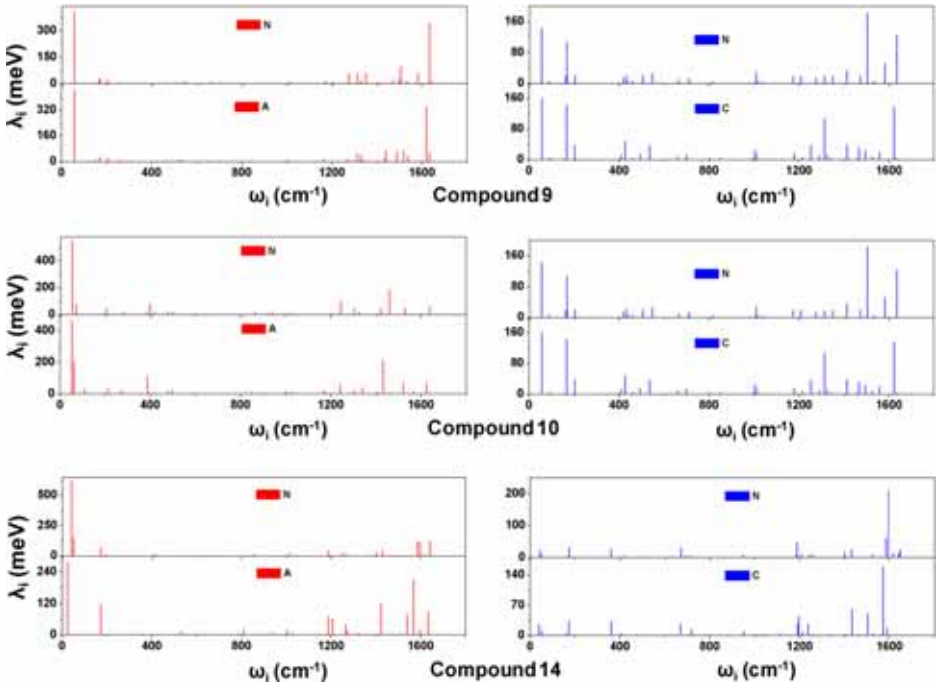

Figure 5. Frequency dependence of reorganization energies for neutral and anionic compound **9** upon electron-transfer process and for neutral and cationic compound **9** upon hole-transfer process (top). Frequency dependence of reorganization energies for neutral and anionic compound **10** upon electron-transfer process and for neutral and cationic compound **10** upon hole-transfer process (middle). Frequency dependence of reorganization energies for neutral and anionic compound **14** upon electron-transfer process and for neutral and cationic compound **14** upon hole-transfer process (below).

molecular axis, contribute 12.2% (0.025 eV) and 10.4% (0.021 eV) to the total λ_h value of compound **2**, while the 1673 cm^{-1} mode in the cation state and the 1592 cm^{-1} mode in the neutral state, which are associated with the stretching vibration of center CC bonds along long and short molecular axis, respectively, contribute 12.7% (0.038 eV) and 9.7% (0.029 eV) to the total λ_h value of compound **1**.

As shown in Table 2, compounds **10** and **14** show obviously smaller λ_h values (0.161 and 0.156 eV) than compound **9** (0.249 eV), although their molecular structures are very similar to each other. The frequency analysis suggests that λ_h values of all three compounds mainly come from the vibration mode(s) corresponding torsion vibration between bilateral and core phenyl rings (see Figure 5). Besides, for compound **9**, the vibration modes associated with CC stretching vibration in core phenyl rings, such as 1622 cm^{-1} in cation state and 1633 cm^{-1} in neutral state, contribute much to λ_h values (0.032 eV), which increase its total λ_h value. In comparison, the contributions of the stretching vibration in core thiophene rings to total λ_h values partly lessen by the attractive interaction between H and S atoms in compounds **10** and **14**; therefore, their λ_h values are smaller than the one of compound **9**. Moreover, it is also found that the λ_e values for these compounds are much larger than their corresponding λ_h values, which suggests that they may be less suitable for n-type semiconductor materials when taking no account of electronic couplings. Comparison of their λ_e values shows that the λ_e value of compound **14** (0.304 eV) is smallest, followed by the one of compound **9** (0.355 eV), and the λ_e value of compound **10** (0.389 eV) is the largest one. From Figure 5, we find that torsion vibrations between bilateral phenyl rings and molecular core plane (<400 cm^{-1}) also contribute much to the λ_e values of compounds **9** and **10**, besides the stretching vibration of chemical bonds in the core part of the molecule, while torsion vibrations contribute very little to the λ_e value of compound **14** due to the strong conjugation effect partly induced by the H···S attractive interaction.

Besides the impact of the edge-core structure on the electronic properties of the materials, it also decides the solid state packing to some extent and further influences the intermolecular orbital overlap between neighboring molecules in organic semiconductors. Considering the fact that the experimental single-crystals of compounds **1**, **2**, and **9** are not reported, here we mainly focus on compounds **10** and **14**, and analyze the influence of the core-edge structure on their molecular stacking mode and intermolecular electronic couplings.

Both molecules **10** and **14** pack in a herringbone geometry in crystals and show six types of intermolecular packing modes as T1, T2, T3, T4, P1, and P2 dimers in the same molecular stacking layer (see Figure 1).[5,8] Symmetrically, dimer P1 was the same as P2, dimer T1 was the same as T3, and dimer T2 was the same as T4, thus only three types of dimers, P1, T1, and T2, needed to be considered in this case. In P1 dimers of compounds **10** and **14**, two monomers parallel each other and show translational symmetry; in this case, the distance between two S atoms in the same monomer largely influence intermolecular interaction because of the intermolecular S···S interaction. As shown in Figure S1 of the Supporting Information, the molecule **10** shows smaller distance between two S atoms in long molecular axis direction than that of compound **14**, and it leads to the stronger repulsion between intermolecular S atoms, which results in larger relative displacement between two monomers along the molecular

DOI: 10.1021/jp5086922
J. Phys. Chem. C 2015, 119, 33−44

axis. Consequently, the electron-transfer integral and hole-transfer integral in the P1 dimer are dramatically decreased due to the reduction in the overall extent of spatial overlap between the two monomers. In comparison, the longer intramolecular S−S distance in molecule **14** decreases the interaction between the intermolecular S atoms in the P1 dimer and furthermore reduce the relative displacement between two monomers along the molecular axis; therefore, compound **14** shows stronger electronic couplings for hole-transfer (19.5 meV) and electron-transfer (22.6 meV) than compound **10**.

In T-type dimers, the electronic couplings are mainly decided by the interaction between the frontier molecular orbitals distributed on the edge part of one monomer and those localized on the center part of the other monomer. Figure 6

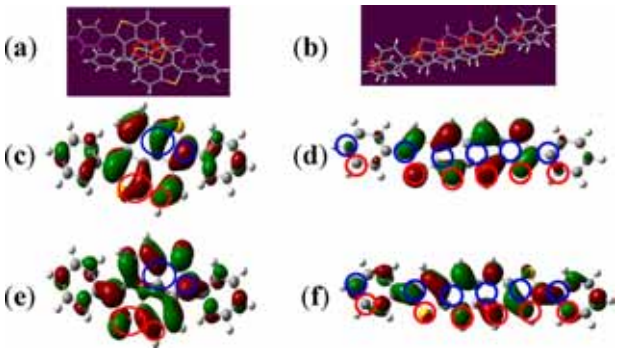

Figure 6. Relative positions of two monomers in T-type dimer for compounds (a) **10** and (b) **14**, and the red circles in (a and b) represent the molecular positions with the smallest distance between two monomers; the red circles and blue circles in (c) HOMOs and (e) LUMOs for compound **10** separately present the molecular positions of upper monomer and lower monomer that corresponds with red circles in (a); and the red and blue circles in (d) HOMOs and (f) LUMOs for compound **14** separately present the molecular positions of upper monomer and lower monomer that corresponds to the red circles in (b).

shows T dimers of compounds **10** and **14**, as well as the interactions between the frontier molecular orbitals. For compound **10**, the relative displacement between two monomers along the molecular axis is much larger because of the repulsive effect between intermolecular S atoms and the steric effect between bilateral benzene rings. In this configuration, the electronic couplings mainly originate from the interactions between the frontier molecular orbitals distributed on C−S/C−C bonds of the upper monomer and the frontier molecular orbitals distributed on C−C bonds of the lower monomer, as shown in Figure 6a. Combined with the HOMO and LUMO orbital charge distributions, it was not surprising that the overlap between the LUMOs or HOMOs leads to significant intermolecular electronic couplings for electron-transfer (45.5 meV) and hole-transfer (43.5 meV), as shown in Figure 6 (panels c and e). Different from compound **10**, the good planarity of compound **14** reduces the steric hindrance between adjacent monomers and leads to small intermolecular displacement. From the relative positions of two monomers in T2 dimers and the distribution characteristics of the HOMOs and LUMOs shown in Figure 6, we can conclude that the electronic couplings in T2 dimers are mainly related with the overlap between the LUMOs/HOMOs localized on the S and C atoms in the thiophene ring. Due to the fact that LUMO orbitals localized on the S atoms much less than HOMO orbitals, the T2 dimer shows much weaker electronic couplings for electron-transfer (16.6 meV) than for hole-transfer (59.1 meV).

3.2. Heteroatom and Substitutents Effects. Heteroatomic substitution is also considered as an important way to improve electronic and charge-transport properties of organic semiconducting materials. In order to elucidate the influence of heteroatomic property on the performances of organic semiconductors, the IPs, EAs, HOMO−LUMO gaps, λ_h and λ_e for compounds **1**, **5**, and **7** were comparatively investigated. As shown in Table 1, the relative ordering of the IPs and HOMO−LUMO gaps for the compounds **1**, **5**, and **7** is as follows: **1** > **7** > **5**; and the ordering of their EAs is **1** < **7** < **5**. It indicates that the decrease of the electronegativity and the increase of the atomic radius for heteroatoms in the same main group are beneficial for improving the field-effect properties, owing to the fact that low IPs and high EAs are favorable for hole- or electron-injection from metallic contacts into the organic semiconductor. Among O, S, and Se atoms, the atomic radius and p-electron energy of O atoms are most close to those of C atoms and thus leads to the highest energy level splitting in the process of bonding; therefore, the hetero-aromatic compound containing O atoms shows lowest HOMO levels, highest LUMO levels, and largest HOMO−LUMO gaps. As the heteroatomic radius and p-electron energies increase, the difference between heteroatoms (S and Se) and C atoms increased gradually, which results in relative lower-energy level splitting and smaller HOMO−LUMO gaps. It well-explains the above observations in IPs, EAs, and LUMO−HOMO gaps.

The calculation results for the reorganization energies of **1**, **5**, and **7** are collected in Table 2, and the analysis of these values shows that the substitution of O atom in the heteroaromatic rings by S or Se atoms induces an obvious decrease in the reorganization energies for the positive polarons; however, the substitution have less influence on the reorganization energies for the negative polarons. This observation is closely related to the different variations in their frontier orbitals. Analyses of the frontier orbitals reveal that heteroatomic substitution contributes more to the HOMOs than to the LUMOs. As shown in Figure S2 of the Supporting Information, the three compounds show very similar local bonding characters in their LUMOs, which suggest that substitution of Se/S for O in furan rings has little influence on the major geometric changes induced by reduction. In comparison, the HOMO distributions of compounds **1**, **5**, and **7** show a significant difference: the nonbonding character becomes evident with the increment of atomic number of heteroatom, and thus we believe that the difference in the λ_h values should be ascribed to the variation of nonbonding character in the HOMOs induced by heteroatomic property. From O to Se, the conjugation degree of heteroatomic rings decrease; however, the percentage of nonbonding character in HOMOs of heteroatomic rings increase with the increase in atomic radius and p-electron energy of heteroatoms, which results in the larger λ_h value of **5** than the ones of **1** and **7**, as well as the larger λ_h value of **7** than that of **1**.

For the compounds **3**, **7** and their related derivatives, the IPs, EAs, HOMO−LUMO gaps, λ_e, and λ_h values are given in Table 1. As expected, the addition of alkyl chains, a weakly electron-donating substituent, created slightly more electron density in the aromatic rings and led to increased repulsive interactions between the electrons and improvement of the HOMO and

DOI: 10.1021/jp5086922
J. Phys. Chem. C 2015, 119, 33−44

LUMO levels but have little influence on HOMO−LUMO gaps. As shown in Table 1, the VIP and VEA of compound **4** is 6.389 and 0.531 eV, respectively, which is slightly lower than the values of unsubstituted **3** (6.593 and 0.573 eV); the VIP and VEA of compound **7** is 7.336 and 0.043 eV, respectively, a little higher than those of compound alkylsubstituted **7** (6.960 and 0.028 eV), while the HOMO−LUMO gaps of **3** (3.59 eV) and **7** (4.27 eV) are very close to those of **4** (3.56 eV) and **8** (4.25 eV), respectively. Furthermore, it is also found that the inclusion of an alkyl substitute leads to a small increase in the λ_h value and decrease in the λ_e value (see Table 2). For the compounds **4** and **8**, the λ_h values were 0.182 and 0.248 eV, respectively, which were considerably larger than those of compounds **3** and **7** (0.176 and 0.229 eV, respectively); the λ_e values for compounds **4** and **8** are 0.208 and 0.301 eV, respectively, whereas the ones of compounds **3** and **7** were slightly larger (0.217 and 0.303 eV, respectively). The observed changes are consistent with the shapes of frontier orbitals of these compounds. For example, the frontier molecular orbitals of molecule **8** (see Figure S3) show that a fraction of HOMOs of alkylsubstituted derivatives localizes on the C−C bonds of alkyl chains, and thus the C−C bond length has to be modified in response to the electronic change when extracting an electron from the HOMO (i.e., oxidation), which has non-negligible contributions to the λ_h value; in contrast, the LUMOs related to the alkyl chains mainly localize on one C atom of alkyl chain and show strong nonbonding character, which induces much less bond length adjustment upon electron-transfer. The slight increase in λ_e values of alkylsubstituted derivatives originates from the fact that the weak electron-donating effect of alkyl groups slightly decreases the electron-dependence of geometric changes.

Moreover, the addition of the alkyl chain also increases the parent molecular volume and H···H repulsive effect between neighboring molecules, which influences the solid state packing motifs of molecular crystals. As shown in Figure S4, both compounds **3** and **4** exhibit a herringbone packing motif dominated by C−H···π interactions; however, their crystals show significant difference in molecular packing architecture parameters. For T dimers, compound **4** shows much larger relative displacement between two neighboring molecules than compound **3**, as the large displacement along the long molecular axis could effectively reduce the H···H repulsive effect induced by alkyl chains. Consequently, T dimers of compound **4** show many weak electronic couplings because of the reduction of spatial overlap between the two monomers. The electronic couplings for hole- and electron-transfer of compound **4** are only 0.25 and 9.06 meV, respectively, which are much smaller than the corresponding values of compound **3** (40.3 and 36.5 meV). For the P dimer, H···H repulsive effect induced by alkyl chains hinders relative slide between two parallel monimers in the long molecular axis direction, and thus, the relative positions of two interacting **4** molecules are closer to perfectly cofacial configurations, which results in the stronger electronic coupling for hole-transfer of compound **4** (60.7 meV) than compound **3** (27.9 meV).

In comparison with the alkyl substitute, the introduction of fused benzene rings and phenyl groups at the longitudinal ends of the parent molecules induces a much-larger decrease in the IP values and increase in the EA values and HOMO−LUMO gaps, which provides a more efficient way to improve the field-effect properties of the organic materials. Significantly, the fusion of benzene rings at longitudinal ends of the parent compound induces higher EAs and lower IPs than the addition of phenyl groups due to their more effective conjunction between the fused benzene rings and parent molecular plane. For example, the VIPs of **9** and **11** are 6.868 and 6.685 eV, respectively, which are 0.47 and 0.65 eV lower, respectively, than that of compound **7**; the EAs of **9** and **11** are 0.601 and 0.833 eV, respectively, which are 0.56 and 0.79 eV higher, respectively, than that of compound **7**. The same conclusion can be obtained from the IPs and EAs of compounds **11**, **12**, and **13**.

The calculation results of the λ_h values and λ_e values (see Table 2) shows that incorporating the phenyl groups pushed the λ_h and λ_e values to be slightly larger than those of the corresponding parent compounds. For the phenyl-substituted **7** (compound **9**), the λ_h and λ_e are 0.250 and 0.354 eV, respectively, which are considerably larger than those of **7** (0.231 and 0.305 eV, respectively); the λ_h and λ_e values of the phenyl-substituted **11** (compound **13**) are 0.149 and 0.218 eV, respectively, whereas those of **11** are slightly smaller (0.136 and 0.208 eV, respectively). These results are attributed to the fact that (i) the introduction of the phenyl groups adds extra rotation degrees of freedom for geometric relaxation into the parent molecule and (ii) intramolecular H−H repulsive interactions weaken the conjugate degree between phenyl groups and parent molecular core, as is discussed in Edge-Core Structure Effects. Quite different from phenyl-substitution, the fusion of benzene rings increases the number of conjugated double bonds in the backbone and extends the effective conjugation length of the systems without introducing the extra rotation degrees of freedom for geometric relaxation. Therefore, the addition of fused benzene rings induced an obvious decrease in the λ_h and λ_e values. For example, the λ_h and λ_e value of compound **11** are 0.136 and 0.208 eV, respectively, as compared to 0.231 and 0.305 eV for unsubstituted **7**; the λ_h and λ_e values of compound **12** are 0.089 and 0.144 eV, respectively, that is, much smaller than those of compound **11**. Combined with the influence of fused benzene rings on IPs and EAs, it can be concluded that the fusion of benzene rings at the longitudinal end is a more useful way to improve the field effect performance.

Figure S4 of the Supporting Information shows the molecular-packing architectures of compounds **11**, **12**, and **13**. It can be seen that compounds **11** and **12** favor face-to-face π-stacked crystal-packing structures, which is usually beneficial for achieving higher carrier mobility, while the X-ray structure of compound **13** exhibits layered herringbone packing, another typical molecular lamella structure. From these structures, we can see that the fusion of benzene rings has little influence on the modes of crystal packing because of their high planarity and C/H ratio. In comparison, incorporating the phenyl groups not only decreases the molecular planarity but also enhances the role of C−H···π interactions in the crystal owing to the increase in the relative C/H ratio, and thus the styrene-substituted oligomers tends to form herringbone packing structure. The calculated electronic couplings for the compounds show that the largest electronic coupling pathways in **11** and **12** come from the P dimers, and the other dimers contribute very little to charge-transfer electronic couplings, suggesting the remarkable anisotropic hole and electron transport mobility of compounds **11** and **12**; for compound **13**, the hole-transfer electronic couplings in T-type dimers and in P-type dimers are very close, while the electron-transfer electronic couplings in T-type dimers are much larger than those in P-type dimers, which

DOI: 10.1021/jp5086922
J. Phys. Chem. C 2015, 119, 33−44

indicates that the hole-transfer and electron-transfer mobilities should possess quite different anisotropic behavior in compound **13**. These characters are consistent with their herringbone packing architectures induced by functionalized modifications.

3.3. Consequences for Carrier Mobility. The drift mobility of the holes/electrons in the studied compounds were estimated from eq 10 by using the reorganization energies and effective electronic coupling matrix elements based on quantum mechanical (QM) calculations. The estimated ranges of the mobility in the same molecular stacking layer are summarized in Table 3. The simulated data for the hole-transfer mobility agree reasonably well with the experimental results under room temperature, suggesting that our computation method and strategy used here are reasonable.

By comparing the simulated electron and hole mobilities of compound **11** and its substituted derivatives (see Table 3), it can be seen that the maximum electron-transfer and hole-transfer mobilities of compound **12** are 5 and 2 times as high as the corresponding maximum values of compound **11**, respectively, which suggests that the fusion of benzene rings improve the charger-carrier mobility of parent compound obviously. In contrast, the addition of phenyl groups induced a decrease in the charge-carrier mobility of the parent compound, especially for the hole-transfer mobility. The maximum hole mobility of compound **13** (phenyl-substituted **11**) is about 0.33 $cm^2\ s^{-1}\ V^{-1}$, only one-seventh of the maximum hole mobility of compound **11** (2.37 $cm^2\ s^{-1}\ V^{-1}$). Additionally, it also can be seen that the charger-carrier mobilities of compound **10** are significantly lower than those of compound **11**, although their molecular structures are very similar to each other. The maximum values of the hole mobility for compound **10** is about 0.13 $cm^2\ s^{-1}\ V^{-1}$, which is one order of magnitude smaller than the corresponding maximum values of hole-transfer mobility for **11**; the maximum values of the electron mobility for compound **10** is about 0.011 $cm^2\ s^{-1}\ V^{-1}$, less than one-sixth of the electron mobility for compound **11**. It is mainly related to the much larger reorganization energies and relatively small V_h values of compound **10**, as shown in Tables 2 and 4.

The mobility anisotropies, which reflects the relative magnitude of electronic couplings in various types of charge-hopping pathways and molecular-packing motifs, are depicted in Figures 7 and 8. From the predicted hole-mobility anisotropic curves for the investigated compounds (Scheme 1), we find that the hole-transfer mobilities could achieve the highest values when the transistor channel orientation was along the P dimers, namely $\Phi = 0°$, except for compounds **6** and **14**. The observation is associated with relative strength of electronic couplings in different dimers and θ_1 values corresponding to T dimers (see Figure 1). As shown in Table 4, the electronic couplings in P-type dimers is much larger than those in T-type dimers for compounds **4**, **5**, **8**, **11**, and **12**, which leads to the largest hole-transfer mobility along P dimers. For compound **13**, the electronic couplings in P dimers is similar to the ones in T dimers; however, the mobility component of μ_T projected to P dimer direction contributes much to the total μ_P due to the small θ_1 value (50.92°) of T dimers. Therefore, compound **13** shows remarkable anisotropic

Table 3. Calculated Electronic Couplings for Hole (V_h) and Electron Transport (V_e) for Different Hopping Pathways in Single Crystals of the Compounds 3, 4, 5, 6, 8, 10, 11, 12, 13, and 14

molecular crystals	dimer types	r (Å)	V_h (meV)	V_e (meV)
3	$P_1 = P_2$	6.658	27.9	17.2
	$T_1 = T_2 = T_3 = T_4$	5.075	40.3	36.5
4	$P_1 = P_2$	5.600	60.7	14.9
	$T_1 = T_2 = T_3 = T_4$	7.183	0.25	9.06
5	$P_1 = P_2$	6.025	88.7	17.8
	$T_1 = T_2 = T_3 = T_4$	5.177	31.9	30.1
6	$P_1 = P_2$	5.886	21.4	59.2
	$T_1 = T_3$	5.017	13.9	2.1
	$T_2 = T_4$	4.921	85.9	29.2
8	$P_1 = P_2$	5.864	59.9	6.64
	$T_1 = T_2 = T_3 = T_4$	4.855	47.1	24.4
10	$P_1 = P_2$	8.818	3.8	6.2
	$T_1 = T_2 = T_3 = T_4$	5.503	43.5	45.5
11	P_1	6.187	71.4	19.6
	P_2	9.848	0.04	0.01
	P_3	7.662	0.20	0.67
	P_4	9.848	1.38	0.28
12	P_1	6.259	70.8	30.3
	P_2	7.569	0.04	0.75
	P_3	9.822	0.04	0.00
	P_4	9.822	1.01	0.12
13	$P_1 = P_2$	6.183	53.5	0.9
	$T_1 = T_2 = T_3 = T_4$	4.904	50.3	35.8
14	$P_1 = P_2$	5.922	19.5	22.6
	$T_1 = T_3$	4.816	61.8	0.62
	$T_2 = T_4$	4.818	59.1	16.6

Table 4. Simulated Hole and Electron Drift Mobilities (μ^- and μ^+) for Compounds 3, 4, 5, 6, 8, 10, 11, 12, 13, and 14 and Part μ^+ Experimental Data at Room Temperature

molecular crystals	μ^-	μ^+	experimental μ^+ (r.t.)
3	0.040−0.048	0.085−0.094	
4	$4.1 \times 10^{-3} \sim 0.011$	$2.8 \times 10^{-10} \sim 0.38$	
5	$8.7 \times 10^{-3} \sim 0.014$	0.011−0.66	0.19−0.20[a]
6	$6.4 \times 10^{-3} \sim 0.24$	0.083−0.15	1.6×10^{-2}[b]
8	$5.3 \times 10^{-3} \sim 9.2 \times 10^{-3}$	0.031−0.11	
10	$8.4 \times 10^{-3} \sim 0.011$	0.11−0.13	6.1×10^{-3}[c]
11	$1.5 \times 10^{-7} \sim 0.071$	$4.8 \times 10^{-7} \sim 2.37$	
12	$1.2 \times 10^{-7} \sim 0.39$	$3.0 \times 10^{-7} \sim 4.53$	$5.3\times 10^{-2} \sim 4.8$, 0.22−0.28, 0.43−0.51[d]
13	0.034−0.052	0.14−0.33	0.7−0.8, 0.44−0.50[e]
14	$1.1 \times 10^{-3} \sim 0.010$	0.19−0.30	[f]

[a]Ref 6. [b]Ref 4. [c]Ref 5. [d]Ref 9. [e]Ref 11. [f]Ref 8.

DOI: 10.1021/jp5086922
J. Phys. Chem. C 2015, 119, 33−44

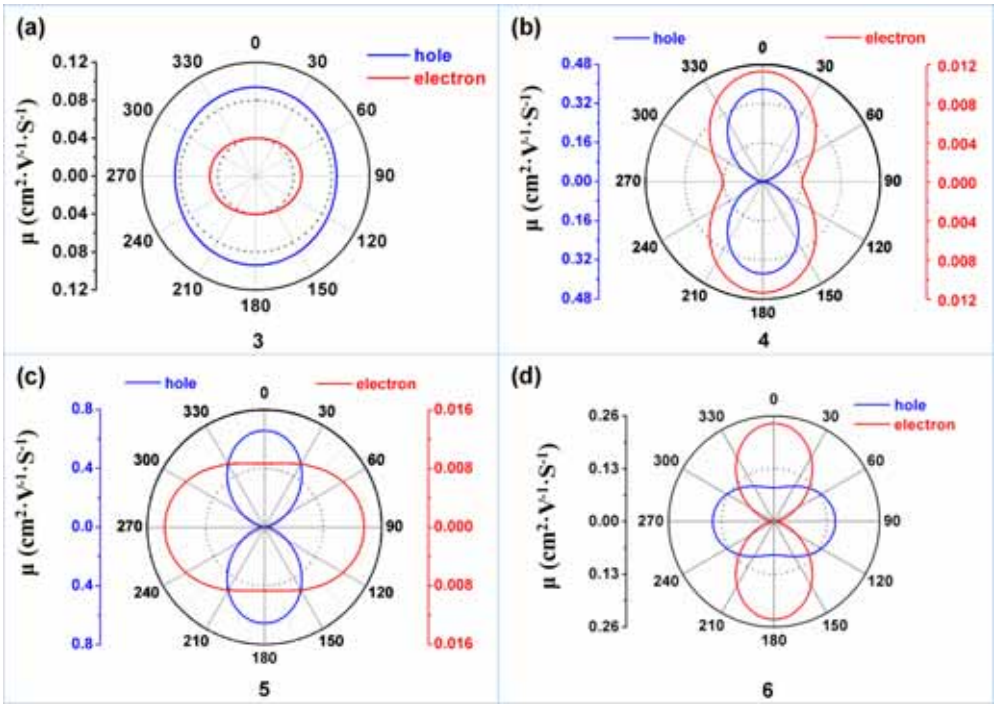

Figure 7. Calculated angle resolved anisotropic hole-mobility (blue line) and electron-mobility (red line) of compound (a) **3** and (d) **6** and calculated angle resolved anisotropic hole-transfer mobility (blue line, and corresponding to left blue coordinate axis) and electron-transfer mobility (red line, and corresponding to right red coordinate axis) of compounds (b) **4** and (c) **5**.

behavior, and the highest and lowest hole mobility directions were along the π-stacking direction and its vertical direction, respectively. For compounds **3** and **10**, although the mobility component of μ_T projected to P dimer direction also contributes much to the μ_P value (θ_1 = 49.008° for **3** and θ_1 = 41.922° for **10**), the much weaker electronic couplings in P dimers seriously affected the total mobility in the P dimer direction, and thus, their anisotropic behaviors are less obvious compared with compound **13**. Different from above compounds, the maximum predicted hole-transfer mobility values of compounds **6** and **14** present at Φ = 90° and the minimum values appear in Φ = 0°, due to the comprehensive effect of weak electronic couplings in P dimers and relatively large θ_1 of T dimers.

The anisotropic electron mobilities in the single crystals are also shown in Figures 7 and 8. From the predicted mobility anisotropy curve we determined that (1) the electron mobilities for **4**, **6**, **10**, **11**, **12**, and **14** could achieve the highest values when the transistor channel orientation is in accord with the direction of P dimers and (2) for **3**, **5**, **8**, and **13**, the highest hole mobility present at Φ = 90°. This is mainly because the maximum V_e values in **4**, **6**, **11**, **12**, and **14** crystals appear in P-type dimers, whereas the maximum V_e values in **3**, **5**, **8**, and **13** crystals appear in T-type dimers. For compound **10**, although the V_e values in P dimers are much weaker than those in T dimers, the small θ_1 value (41.922°, less than 45°) induces larger mobility component of μ_T at Φ = 0° than that at Φ = 90°, which well rationalizes the anisotropic behavior of compound **10**. Our anisotropic electron mobilities here provide a guide for the optimization OTFT/OFET performance and improvement of their durability.

4. CONCLUSIONS

In conclusion, the electronic and charge transport properties of BTBT and its derivatives/analogues have been investigated. Our results showed that (1) the electronic properties, reorganization energies, and the molecular arrangement in the single crystals can be optimized by designing reasonable edge-core structures, which influences the frontier molecular orbital charge distributions and the steric hindrance in the solid state; (2) the introduction of phenyl groups in molecules **7** and **11** can decrease the hole-transfer reorganization energy to some content but increase the electron-transfer reorganization energy and change the molecular arrangement from π stacking to herringbone packing, resulting in the decreased charger-transfer mobility; in comparison, the fusion of benzene rings at longitudinal end of molecule **11** effectively decrease the electron-transfer and hole-transfer reorganization energies and has little influence on the modes of crystal packing, and thus the charger-transfer mobility of molecular **12** was highly improved compared with **11**; and (3) heteroatom substitution changes not only the conjugation degree of the molecular core plane but also the local bonding characters between neighboring atoms, which well explains the decrease in hole-transfer reorganization energy with the increment of atomic number of heteroatom (O, S, and Se). Furthermore, we also simulated their angular resolution anisotropic mobility for both electron- and hole-transport and provides a guide for the optimization OTFT/OFET performance by analyzing the relationship between conducting channels of electronic device and molecular crystal structures.

DOI: 10.1021/jp5086922
J. Phys. Chem. C 2015, 119, 33−44

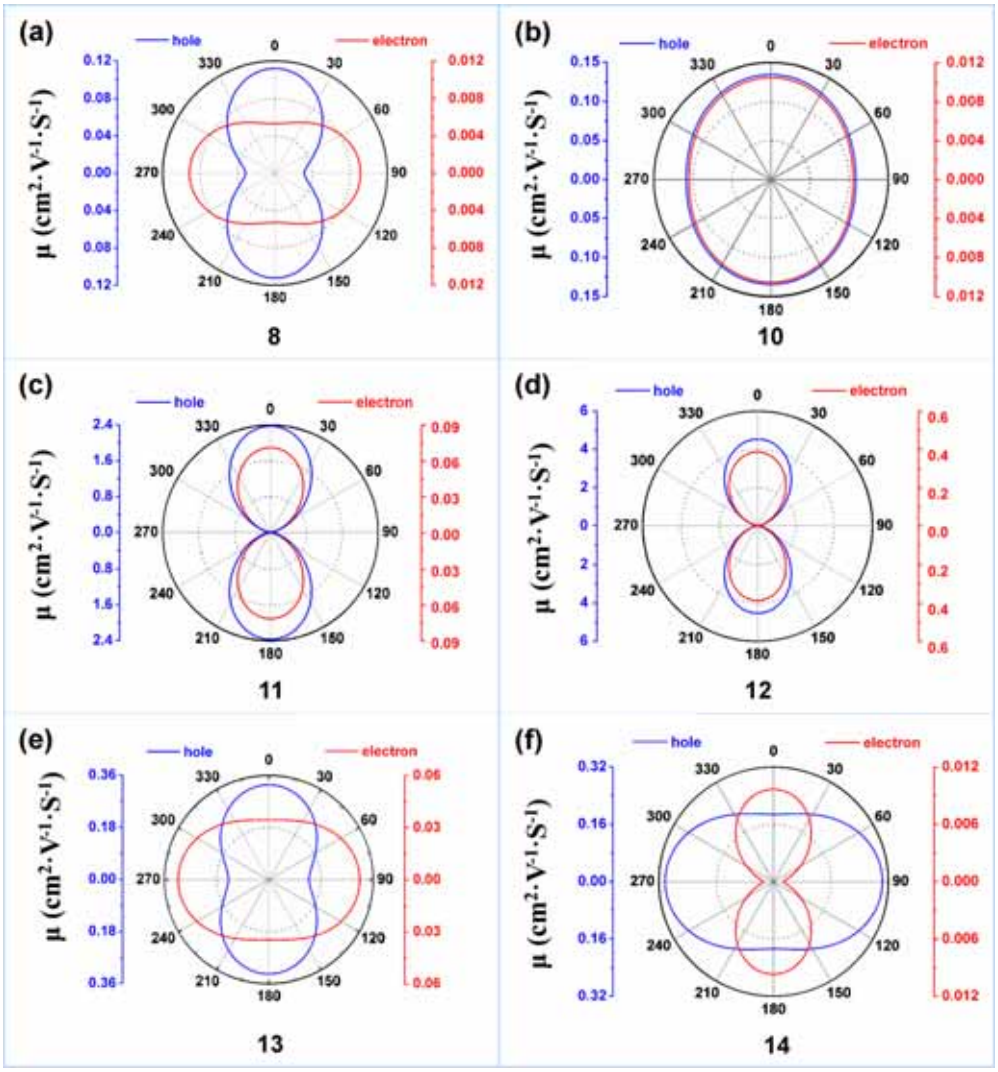

Figure 8. Calculated angle resolved anisotropic hole-mobility (blue line, and corresponding to left blue coordinate axis) and electron-mobility (red line, and corresponding to right red coordinate axis) of compounds (a) **8**, (b) **10**, (c) **11**, (d) **12**, (e) **13**, and (f) **14**.

■ ASSOCIATED CONTENT

Supporting Information

The molecular packing architectures of compounds **3**, **4**, **10**, **11**, **12**, **13**, **14** (Figures S1 and S4) and the frontier molecular orbitals for compounds **1**, **5**, **7**, and **8** (Figures S2 and S3). This material is available free of charge via the Internet at http://pubs.acs.org.

■ AUTHOR INFORMATION

Corresponding Authors

*E-mail: huipeng_ma@126.com. Tel: +86 41186110391.
*E-mail: dong@d lnu.edu.cn. Tel: +86 41187556959.

Notes

The authors declare no competing financial interest.

■ ACKNOWLEDGMENTS

This work is supported by the 973 Program (Grant No. 2012CB626801), National Natural Science Foundation of China (Grant No. 11274057, 11474046, 11304029), Program for New Century Excellent Talents in University (Grant No. NCET-13-0702), Science and Technology Project of Liaoning Province (Grant No. 2012222009), Science and Technique Foundation of Dalian (Grant No. 2012J21DW016, 2013A14GX040), and the Initial Funds for Imported Talents' Research Projects, Dalian Nationalities University (Grant 20136131). We are grateful to Prof. Reimers for providing us with the DUSHIN code.

■ REFERENCES

(1) Reineke, S.; Thomschke, M.; Lussem, B.; Leo, K. White Organic Light-Emitting Diodes: Status and Perspective. *Rev. Mod. Phys.* **2013**, *85*, 1245−1293.
(2) Mei, J. G.; Diao, Y.; Appleton, A. L.; Fang, L.; Bao, Z. N. Integrated Materials Design of Organic Semiconductors for Field-Effect Transistors. *J. Am. Chem. Soc.* **2013**, *135*, 6724−6746.
(3) Myers, J. D.; Xue, J. G. Organic Semiconductors and their Applications in Photovoltaic Devices. *Polym. Rev.* **2012**, *52*, 1−37.
(4) Takimiya, K.; Kunugi, Y.; Konda, Y.; Niihara, N.; Otsubo, T. 2,6-Diphenylbenzo 1,2-b: 4,5-b' Dichalcogenophenes: A New Class of High-performance Semiconductors for Organic Field-Effect Transistors. *J. Am. Chem. Soc.* **2004**, *126*, 5084−5085.

DOI: 10.1021/jp5086922
J. Phys. Chem. C 2015, 119, 33−44

(5) Takimiya, K.; Kunugi, Y.; Toyoshima, Y.; Otsubo, T. 2,6-Diarylnaphtho 1,8-bc: 5,4-b'c' Dithiophenes as New High-Performance Semiconductors for Organic Field-Effect Transistors. *J. Am. Chem. Soc.* **2005**, *127*, 3605−3612.
(6) Takimiya, K.; Kunugi, Y.; Konda, Y.; Ebata, H.; Toyoshima, Y.; Otsubo, T. 2,7-Diphenyl[1]Benzoselenopheno[3,2-b][1]-Benzoselenophene as a Stable Organic Semiconductor for a High-Performance Field-Effect Transistor. *J. Am. Chem. Soc.* **2006**, *128*, 3044−3050.
(7) Takimiya, K.; Ebata, H.; Sakamoto, K.; Izawa, T.; Otsubo, T.; Kunugi, Y. 2,7-Diphenyl[1]Benzothieno[3,2-b]Benzothiophene, a New Organic Semiconductor for Air-Stable Organic Field-Effect Transistors with Mobilities up to 2.0 cm^2 V^{-1} s^{-1}. *J. Am. Chem. Soc.* **2006**, *128*, 12604−12605.
(8) Shinamura, S.; Osaka, I.; Miyazaki, E.; Nakao, A.; Yamagishi, M.; Takeya, J.; Takimiya, K. Linear- and Angular-Shaped Naphthodithiophenes: Selective Synthesis, Properties, and Application to Organic Field-Effect Transistors. *J. Am. Chem. Soc.* **2011**, *133*, 5024−5035.
(9) Niimi, K.; Shinamura, S.; Osaka, I.; Miyazaki, E.; Takimiya, K. Dianthra 2,3-*b*:2'3'-*f*]thieno[3,2-*b*]thiophene (DATT): Synthesis, Characterization, and FET Characteristics of New pi-Extended Heteroarene with Eight Fused Aromatic Rings. *J. Am. Chem. Soc.* **2011**, *133*, 8732−8739.
(10) Mitsui, C.; Soeda, J.; Miwa, K.; Tsuji, H.; Takeya, J.; Nakamura, E. Naphtho[2,1-*b*:6,5-*b*′]difuran: A Versatile Motif Available for Solution-Processed Single-Crystal Organic Field-Effect Transistors with High Hole Mobility. *J. Am. Chem. Soc.* **2012**, *134*, 5448−5451.
(11) Kang, M. J.; Miyazaki, E.; Osaka, I.; Takimiya, K.; Nakao, A. Diphenyl Derivatives of Dinaphtho[2,3-b:2′,3′-*f*]thieno[3,2-*b*]-thiophene: Organic Semiconductors for Thermally Stable Thin-Film Transistors. *ACS Appl. Mater. Interfaces* **2013**, *5*, 2331−2336.
(12) Ebata, H.; Izawa, T.; Miyazaki, E.; Takimiya, K.; Ikeda, M.; Kuwabara, H.; Yui, T. Highly Soluble [1]Benzothieno[3,2-b]-Benzothiophene (BTBT) Derivatives for High-Performance, Solution-Processed Organic Field-Effect Transistors. *J. Am. Chem. Soc.* **2007**, *129*, 15732−15733.
(13) Norton, J. E.; Bredas, J.-L. Polarization Energies in Oligoacene Semiconductor Crystals. *J. Am. Chem. Soc.* **2008**, *130*, 12377−12384.
(14) Yin, S.; Li, L.; Yang, Y.; Reimers, J. R. Challenges for the Accurate Simulation of Anisotropic Charge Mobilities through Organic Molecular Crystals: The beta Phase of mer-Tris(8-hydroxyquinolinato)aluminum(III) (Alq3) Crystal. *J. Phys. Chem. C* **2012**, *116*, 14826−14836.
(15) Reimers, J. R. A Practical Method for the Use of Curvilinear Coordinates in Calculations of Normal-Mode-Projected Displacements and Duschinsky Rotation Matrices for Large Molecules. *J. Chem. Phys.* **2001**, *115*, 9103−9109.
(16) Frisch, M. J.; Trucks, G. W.; Schlegel, H. B.; Scuseria, G. E.; Robb, M. A.; Cheeseman, J. R.; Montgomery, J. A., Jr.; Vreven, T.; Kudin, K. N.; Burant, J. C., and et al.; *Gaussian 03*, revision C.02; Gaussian, Inc.; Wallingford, CT, 2004.
(17) te Velde, G.; Bickelhaupt, F. M.; Baerends, E. J.; Guerra, C. F.; Van Gisbergen, S. J. A.; Snijders, J. G.; Ziegler, T. Chemistry with ADF. *J. Comput. Chem.* **2001**, *22*, 931−967.
(18) Wen, S.-H.; Li, A.; Song, J.; Deng, W.-Q.; Han, K.-L.; Goddard, W. A., III First-Principles Investigation of Anistropic Hole Mobilities in Organic Semiconductors. *J. Phys. Chem. B* **2009**, *113*, 8813−8819.
(19) Huang, J.-D.; Wen, S.-H.; Deng, W.-Q.; Han, K.-L. Simulation of Hole Mobility in α-Oligofuran Crystals. *J. Phys. Chem. B* **2011**, *115*, 2140−2147.
(20) Han, K.; Huang, J.; Chai, S.; Wen, S.; Deng, W. Anisotropic Mobilities in Organic Semiconductors. *Protocol Exchange* **2013**, DOI: doi:10.1038/protex.2013.070.
(21) Chai, S.; Wen, S.-H.; Han, K.-L. Understanding Electron-Withdrawing Substituent Effect on Structural, Electronic and Charge Transport Properties of Perylene Bisimide Derivatives. *Org. Electron.* **2011**, *12*, 1806−1814.
(22) Chai, S.; Wen, S.-H.; Huang, J.-D.; Han, K.-L. Density Functional Theory Study on Electron and Hole Transport Properties of Organic Pentacene Derivatives with Electron-Withdrawing Substituent. *J. Comput. Chem.* **2011**, *32*, 3218−3225.
(23) Huang, J.-D.; Wen, S.-H.; Han, K.-L. First-Principles Investigation of the Electronic and Conducting Properties of Oligothienoacenes and Their Derivatives. *Chem.—Asian J.* **2012**, *7*, 1032−1040.
(24) Huang, J. D.; Wen, S. H. First-Principles Investigation of Anisotropic Electron and Hole Mobility in Heterocyclic Oligomer Crystals. *ChemPhysChem* **2013**, *14*, 2579−2588.
(25) Anthony, J. E.; Facchetti, A.; Heeney, M.; Marder, S. R.; Zhan, X. n-Type Organic Semiconductors in Organic Electronics. *Adv. Mater.* **2010**, *22*, 3876−3892.
(26) Wu, W.; Liu, Y.; Zhu, D. pi-Conjugated Molecules with Fused Rings for Organic Field-Effect Transistors: Design, Synthesis and Applications. *Chem. Soc. Rev.* **2010**, *39*, 1489−1502.
(27) Usta, H.; Facchetti, A.; Marks, T. J. n-Channel Semiconductor Materials Design for Organic Complementary Circuits. *Acc. Chem. Res.* **2011**, *44*, 501−510.

DOI: 10.1021/jp5086922
J. Phys. Chem. C 2015, 119, 33−44